Measurement of the cross section of $e^+e^- \to \Xi^-\bar{\Xi}^+$ at center-of-mass energies between 3.510 and 4.843 GeV

The BESIII collaboration

E-mail: besiii-publications@ihep.ac.cn

ABSTRACT: Using e^+e^- collision data corresponding to a total integrated luminosity of $12.9\,\mathrm{fb}^{-1}$ collected with the BESIII detector at the BEPCII collider, the exclusive Born cross sections and the effective form factors of the reaction $e^+e^- \to \Xi^-\bar{\Xi}^+$ are measured via the single baryon-tag method at 23 center-of-mass energies between 3.510 and 4.843 GeV. Evidence for the decay $\psi(3770) \to \Xi^-\bar{\Xi}^+$ is observed with a significance of 4.5σ by analyzing the measured cross sections together with earlier BESIII results. For the other charmonium(-like) states $\psi(4040)$, $\psi(4160)$, $Y(4230)$, $Y(4360)$, $\psi(4415)$, and $Y(4660)$, no significant signal of their decay to $\Xi^-\bar{\Xi}^+$ is found. For these states, upper limits of the products of the branching fraction and the electronic partial width at the 90% confidence level are provided.

Contents

1 Introduction

Below the open-charm threshold, the mass spectrum of the conventional charmonium states is well matched to the predictions from the potential quark model [1]. Above the open-charm threshold, this model predicts five vector charmonium states between the threshold and $4.9 \, \text{GeV}/c^2$, namely, the $3S$, $2D$, $4S$, $3D$, and $5S$ states. However, an overpopulation of vector states has been observed in this energy region. Three of them, $\psi(4040)$, $\psi(4160)$, $\psi(4415)$, are dominated by open-charm final states [2]. Other states, e.g. $Y(4230)$, $Y(4260)$, $Y(4360)$, $Y(4634)$, $Y(4660)$, are mainly observed in hidden-charm final states, produced via initial state radiation (ISR) processes at BABAR and Belle [3–11] or via direct production processes at CLEO [12] and BESIII [13, 14]. These Y states cannot be easily accommodated in the charmonium spectrum predicted in the quark model, and many hypotheses have been

proposed to interpret them [15–23], such as hybrids, multiple-quark states, molecules, etc. However, no solid conclusion can be made at present and puzzles remain for these vector charmonium(-like) states.

This situation reflects the present insufficient understanding of the strong interaction, especially in the non-perturbative regime. To improve the situation, additional experimental measurements are desirable. Among these measurements, the decays of $\psi/Y \to$ light baryon-antibaryon($B\bar{B}$) are promising due to the simple topologies of the final states and relatively well understood mechanisms, dominated by three-gluons or one-photon processes. Moreover, measurements of electromagnetic form factors and effective form factors of the $B\bar{B}$ pairs may provide insight into the internal structure of the charmonium(-like) states. Up to now the experimental information on $B\bar{B}$ decays of these charmonium-(like) states is scarce above the open-charm threshold. Although many experimental studies [7, 24–30] of $B\bar{B}$ pair production are performed in this energy region by the BESIII and Belle experiments, no $B\bar{B}$ decays of the vector charmonium(-like) states have been observed except for the evidence of $\psi(3770) \to \Lambda\bar{\Lambda}$. It could indicate that the production of $\Xi^-\bar{\Xi}^+$ mainly proceeds through the continuum process and not through charmonium resonances, justifying the assumption of one-photon production. Thus, more precise measurements of exclusive cross sections of $e^+e^- \to B\bar{B}$ final states above the open-charm threshold could provide a valuable information to understand the nature of these vector charmonium(-like) states.

In this article, measurements of the Born cross section and the effective form factor for the process $e^+e^- \to \Xi^-\bar{\Xi}^+$ are presented using data corresponding to a total integrated luminosity of $12.9\,\text{fb}^{-1}$ collected at center-of-mass (CM) energies $\sqrt{s}$ between 3.510 and 4.843 GeV with the BESIII detector [31] at the BEPCII collider [32]. In addition, potential contributions from resonances are studied by fitting the dressed cross section of the $e^+e^- \to \Xi^-\bar{\Xi}^+$ reaction combined with the earlier BESIII results reported in 2020 [26].

2 BESIII detector and Monte Carlo simulation

The BESIII detector [31] records symmetric e^+e^- collisions provided by the BEPCII storage ring [32] in the CM energy range from 2.0 to 4.95 GeV, with a peak luminosity of $1 \times 10^{33}\,\text{cm}^{-2}\,\text{s}^{-1}$ achieved at $\sqrt{s} = 3.77$ GeV. BESIII has collected large data samples in this energy region [33–35]. The cylindrical core of the BESIII detector covers 93% of the full solid angle and consists of a helium-based multilayer drift chamber (MDC), a plastic scintillator time-of-flight system (TOF), and a CsI(Tl) electromagnetic calorimeter (EMC), which are all enclosed in a superconducting solenoidal magnet providing a 1.0 T magnetic field. The solenoid is supported by an octagonal flux-return yoke with resistive plate counter muon identification modules interleaved with steel. The charged-particle momentum resolution at $1\,\text{GeV}/c$ is 0.5%, and the dE/dx resolution is 6% for electrons from Bhabha scattering. The EMC measures photon energies with a resolution of 2.5% (5%) at 1 GeV in the barrel (end cap) region. The time resolution in the TOF barrel region is 68 ps, while that in the end cap region is 110 ps. The end cap TOF system was upgraded in 2015 using multigap resistive plate chamber technology, providing a time resolution of 60 ps, which benefits 77% of the data used in this analysis [36–38].

Simulated data samples produced with a GEANT4-based [39] Monte Carlo (MC) package, which includes the geometric description of the BESIII detector [40] and the detector response, are used to determine the signal detection efficiency. A sample of 200,000 $e^+e^- \to \Xi^-\bar{\Xi}^+$ events is simulated with a uniform phase space (PHSP) distribution for each of the 23 CM energy points in the range from 3.510 to 4.843 GeV. The decay chain of the Ξ^- baryon is handled by the EVTGEN program [41, 42] using a PHSP model. The production process is simulated by the KKMC generator [43] that includes the beam energy spread and ISR in the e^+e^- annihilation.

3   Event selection

The selection of $e^+e^- \to \Xi^-\bar{\Xi}^+$ events with a full reconstruction method suffers from low reconstruction efficiency. Therefore, a partial reconstruction technique is employed, in which only the Ξ^- baryon is reconstructed via its decay $\Xi^- \to \Lambda\pi^-$ with the subsequent decay $\Lambda \to p\pi^-$, and the presence of the $\bar{\Xi}^+$ anti-baryon is inferred from the system recoiling against the reconstructed Ξ^-. Unless otherwise noted, the charge conjugated state is implicitly included throughout this paper.

Tracks of charged particles detected in the MDC are required to be within the optimal MDC angular coverage, $|\cos\theta| < 0.93$, where the polar-angle θ is defined with respect to the MDC symmetry axis. At least one positively charged and two negatively charged tracks are required, which are required to be well reconstructed in the MDC with good helix fits. The particle identification (PID) for charged particles combines measurements of the $\mathrm{d}E/\mathrm{d}x$ by the MDC and the time of flight by the TOF to form likelihoods $\mathcal{L}(h)$ ($h = p, K, \pi$) for each hadron hypothesis h. Tracks are identified as protons if the proton hypothesis has the greatest likelihood ($\mathcal{L}(p) > \mathcal{L}(K)$ and $\mathcal{L}(p) > \mathcal{L}(\pi)$), while charged pions are identified by requiring that $\mathcal{L}(\pi) > \mathcal{L}(p)$ and $\mathcal{L}(\pi) > \mathcal{L}(K)$. Only events with at least two negatively charged pions and one proton are kept for the further analysis.

The reconstruction of Λ and Ξ^- baryons follows refs. [44–47]. Briefly, to reconstruct Λ candidates and suppress non-Λ background, a secondary vertex fit [48] is applied to all $p\pi^-$ combinations, and their invariant mass is required to be within $5\,\mathrm{MeV}/c^2$ from the known Λ mass. The selection window is determined by optimizing a figure of merit (FOM) defined as $S/\sqrt{S+B}$, where S is the number of signal MC events and B is the number of the background events expected from simulation. Similarly, the Ξ^- candidates are reconstructed using a further secondary vertex fit applied to the combination of the selected π^- and Λ candidates which minimizes the difference $|M_{\pi^-\Lambda} - m_{\Xi^-}|$, where $M_{\pi^-\Lambda}$ is the invariant mass of the $\pi^-\Lambda$ combination and m_{Ξ^-} is the known mass of Ξ^- from the Particle Data Group (PDG) [49]. The signal window is defined by requiring that $M_{\pi^-\Lambda}$ is within $10\,\mathrm{MeV}/c^2$ from the known Ξ^- mass. This width of the window is determined by optimizing the FOM and is about three times the experimental mass resolution. The decay length of the Ξ^- candidate, i.e. the distance between the average position of the e^+e^- collisions and the decay vertex of Ξ^-, is required to be greater than zero. The decay length of the Λ candidate is also required to be greater than zero.

To extract anti-baryon $\bar{\Xi}^+$ candidates, we calculate the mass recoiling against the selected $\pi^-\Lambda$ system as

$$M_{\pi^-\Lambda}^{\text{recoil}} = \sqrt{\left(\sqrt{s} - E_{\pi^-\Lambda}\right)^2 - \vec{p}_{\pi^-\Lambda}^{\,2}}, \qquad (3.1)$$

where $E_{\pi^-\Lambda}$ and $\vec{p}_{\pi^-\Lambda}$ are the energy and momentum of the selected $\pi^-\Lambda$ candidates in the CM frame, and $\sqrt{s}$ is the CM energy. The signal window is defined by requiring that $M_{\pi^-\Lambda}^{\text{recoil}}$ is within $60\,\text{MeV}/c^2$ from the known Ξ^- mass. Figure 1 shows the scatter plots of $M_{\pi^-\Lambda}$ versus $M_{\pi^-\Lambda}^{\text{recoil}}$ for each energy point separately and for the sum of all energy points. A clear cluster of events around the nominal Ξ^- mass can be seen.

4 Born cross section measurement

4.1 Extraction of signal yields

After applying the above selection criteria, the surviving background events are mainly from non-$\Xi^-\bar{\Xi}^+$ events, such as $e^+e^- \to \pi^+\pi^-\Lambda\bar{\Lambda}$. The background yield in the signal region is estimated using four sideband regions B_i, where $i = 1, 2, 3, 4$, each with the same area as the signal region. The regions are shown in figure 1, and the exact ranges are defined by

- B_1: $M_{\pi^-\Lambda} \in [1.282, 1.302]\,\text{GeV}/c^2$ & $M_{\pi^-\Lambda}^{\text{recoil}} \in [1.442, 1.562]\,\text{GeV}/c^2$,

- B_2: $M_{\pi^-\Lambda} \in [1.342, 1.362]\,\text{GeV}/c^2$ & $M_{\pi^-\Lambda}^{\text{recoil}} \in [1.442, 1.562]\,\text{GeV}/c^2$,

- B_3: $M_{\pi^-\Lambda} \in [1.342, 1.362]\,\text{GeV}/c^2$ & $M_{\pi^-\Lambda}^{\text{recoil}} \in [1.082, 1.202]\,\text{GeV}/c^2$,

- B_4: $M_{\pi^-\Lambda} \in [1.282, 1.302]\,\text{GeV}/c^2$ & $M_{\pi^-\Lambda}^{\text{recoil}} \in [1.082, 1.202]\,\text{GeV}/c^2$.

The signal yield N_{obs} for the $e^+e^- \to \Xi^-\bar{\Xi}^+$ reaction at each energy point can then be determined by subtracting the number of events in the sideband regions from the signal region, i.e. $N_{\text{obs}} = N_S - N_{\text{bkg}}$, where N_S is number of events in the signal region, $N_{\text{bkg}} = \frac{1}{4}\sum_{i=1}^{4} B_i$. The signal yields are listed in table 1. The single baryon-tag method leads to a double counting effect for the $\Xi^-\bar{\Xi}^+$ final state, which is taken into account in the calculation of the statistical uncertainty based on the study of MC simulation [26]. This does not affect the central value of the final result but it requires a correction of the statistical uncertainty, which is underestimated by approximately 12%.

4.2 Determination of the Born cross section

The Born cross section for the $e^+e^- \to \Xi^-\bar{\Xi}^+$ process at a given CM energy is calculated as

$$\sigma^B = \frac{N_{\text{obs}}}{2 \cdot \mathcal{L} \cdot (1+\delta) \cdot \frac{1}{|1-\Pi|^2} \cdot \epsilon \cdot \mathcal{B}(\Xi^- \to \pi^-\Lambda) \cdot \mathcal{B}(\Lambda \to p\pi^-)}, \qquad (4.1)$$

where N_{obs} is the number of the observed signal events, a factor of 2 represents the charge conjugate mode included, $\mathcal{L}$ is the integrated luminosity, $(1+\delta)$ is the ISR correction factor, $\frac{1}{|1-\Pi|^2}$ is the vacuum polarization (VP) correction factor, ϵ is the detection efficiency, while $\mathcal{B}(\Xi^- \to \pi^-\Lambda)$ and $\mathcal{B}(\Lambda \to p\pi^-)$ are the corresponding branching fractions taken from the
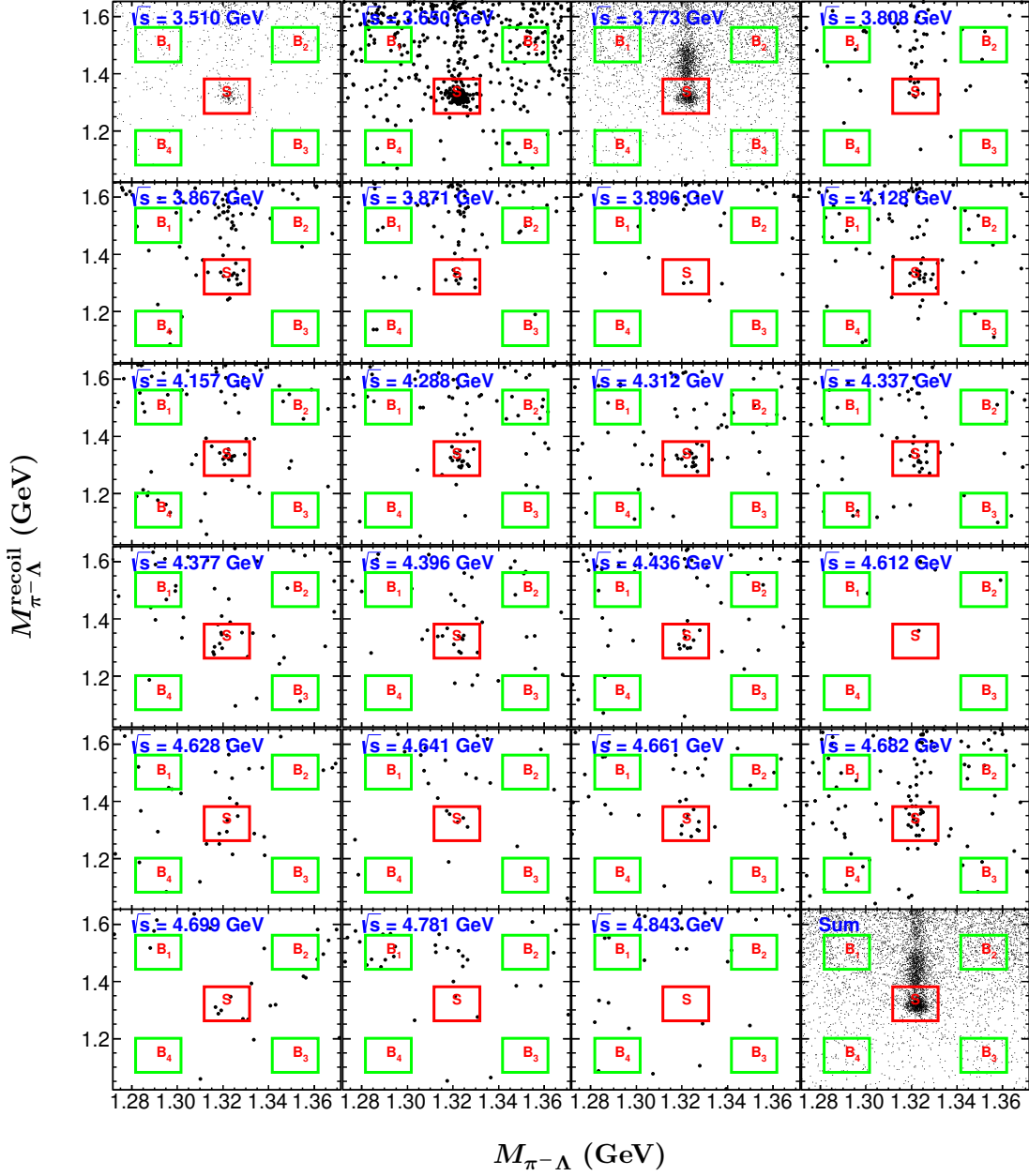
Figure 1. Distributions of $M_{\pi^-\Lambda}$ versus $M_{\pi^-\Lambda}^{\mathrm{recoil}}$ for each energy point and for the sum of all energy points (bottom, right) between 3.510 and 4.843 GeV from data. The red boxes represent the signal regions and the green boxes represent the selected sideband regions.

$\sqrt{s}$ (GeV)	N_S	N_{bkg}	N_{obs} (N^{UL})	$\mathcal{S}$ (σ)
3.510	143.0	18.5	$124.5^{+12.8}_{-11.1}$	10.4
3.650	144.0	11.5	$132.5^{+12.8}_{-11.2}$	11.0
3.773	703.0	100.8	$602.2^{+27.7}_{-25.4}$	22.7
3.808	8.0	1.8	$6.2^{+4.0}_{-1.7}$ (<13.2)	2.2
3.867	12.0	1.0	$11.0^{+3.8}_{-3.1}$	3.2
3.871	9.0	2.0	$7.0^{+3.3}_{-2.7}$ (<13.4)	2.3
3.896	2.0	0.2	$1.8^{+2.0}_{-0.9}$ (<5.4)	1.2
4.128	18.0	2.8	$15.2^{+5.4}_{-3.1}$	3.6
4.157	14.0	3.2	$10.8^{+4.3}_{-3.2}$ (<18.8)	2.9
4.288	19.0	2.2	$16.8^{+4.9}_{-3.8}$	3.8
4.312	17.0	1.5	$15.5^{+5.0}_{-3.3}$	3.8
4.337	16.0	1.8	$14.2^{+5.1}_{-2.9}$	3.6
4.377	11.0	1.5	$9.5^{+4.2}_{-2.5}$ (<16.8)	2.9
4.396	11.0	0.5	$10.5^{+4.2}_{-2.5}$	3.2
4.436	9.0	1.0	$8.0^{+3.3}_{-2.7}$ (<14.3)	2.7
4.612	1.0	0.5	$0.5^{+1.9}_{-0.2}$ (<3.7)	0.5
4.628	4.0	1.2	$2.8^{+2.5}_{-1.5}$ (<7.5)	1.4
4.641	6.0	0.0	$6.0^{+2.8}_{-2.1}$ (<11.1)	2.4
4.661	9.0	1.0	$8.0^{+3.3}_{-2.7}$ (<14.3)	2.7
4.682	16.0	3.8	$12.2^{+5.1}_{-2.9}$	3.1
4.699	6.0	0.5	$5.5^{+3.3}_{-1.6}$ (<11.1)	2.2
4.781	2.0	1.5	$0.5^{+2.3}_{-0.5}$ (<4.6)	0.4
4.843	0.0	0.8	$-0.8^{+1.7}_{-0.8}$ (<2.0)	0.0

Table 1. Number of signal (N_S) and background (N_{bkg}) events for each energy points. The upper limits (N^{UL}) at the 90% confidence level including the systematic uncertainty, and the statistical uncertainties for the observed events are determined by the TRolke method with Poisson background and Gaussian efficiency model [50]. The signal significance ($\mathcal{S}$) is estimated as $N_S/\sqrt{N_S + N_{\mathrm{bkg}}}$.

world average [49]. The ISR correction factor is obtained using the QED calculation as described in ref. [51]. The VP correction factor is calculated according to ref. [52]. The Born cross section is not well determined beforehand, thus an iterative weighting method for updating the efficiency and ISR correction factor is used as proposed in ref. [53]. This procedure is repeated until the difference of $(1 + \delta)\epsilon$ between iterations is less than 0.5%. The efficiency, ISR correction factor, and Born cross section of the last round are accepted as the final results. The measured cross sections for each energy point together with the CLEO-c results at $\sqrt{s} = 3.770$ and $4.160\,\mathrm{GeV}$ [54] are shown in figure 2.

5 Determination of the effective form factor

Under the assumption that the dominant process is one-photon exchange $e^+e^- \to \gamma^* \to \Xi^-\bar{\Xi}^+$, one can parameterize the differential cross section in terms of electric and magnetic form factors G_E and G_M. These are assumed to be continuous functions of the momentum transfer squared, $s = q^2$. The differential cross section can be written [55] as

$$\frac{d\sigma^B(s)}{d\Omega} = \frac{\alpha^2\beta C}{4s}\left[|G_M(s)|^2(1+\cos^2\theta) + \frac{1}{\tau}|G_E(s)|^2\sin^2\theta\right], \tag{5.1}$$

where s is the square of the CM energy, α is the fine structure constant, the variable $\beta = \sqrt{1 - \frac{1}{\tau}}$ is the velocity, $\tau = \frac{s}{4m_{\Xi^-}^2}$, and the Coulomb correction factor C [55, 56] parameterizes the electromagnetic interaction between the outgoing baryon and anti-baryon. For neutral baryons, the Coulomb factor is unity, while for point-like charged fermions $C = \frac{\pi\alpha}{\beta} \cdot \frac{\sqrt{1-\beta^2}}{1-e^{-\frac{\pi\alpha}{\beta}}}$ [57–60]. Similarly, the Born cross section can be derived by integrating over the full solid angle as

$$\sigma^B(s) = \frac{4\pi\alpha^2 C\beta}{3s}\left[|G_M(s)|^2 + \frac{1}{2\tau}|G_E(s)|^2\right]. \tag{5.2}$$

Furthermore, we define the effective form factor $G_{\text{eff}}(s)$ as a linear combination of the electric and magnetic form factors as

$$|G_{\text{eff}}(s)| = \sqrt{\frac{2\tau|G_M(s)|^2 + |G_E(s)|^2}{2\tau + 1}}, \tag{5.3}$$

which can be transformed to

$$|G_{\text{eff}}(s)| = \sqrt{\frac{3s\sigma^B}{4\pi\alpha^2 C\beta\left(1 + \frac{2m_{\Xi^-}^2}{s}\right)}}, \tag{5.4}$$

and its uncertainty is propagated to be

$$\delta_{|G_{\text{eff}}(s)|} = \frac{1}{2}C'\sqrt{\frac{1}{\sigma^B}} \cdot \delta_{\sigma^B}, \tag{5.5}$$

where δ_{σ^B} is the uncertainty of the Born cross section and

$$C' = \sqrt{\frac{3s}{4\pi\alpha^2 C\beta\left(1 + \frac{2m_{\Xi^-}^2}{s}\right)}}, \tag{5.6}$$

where m_{Ξ^-} is the Ξ^- baryon mass. The results for the effective form factors at each energy point are shown in figure 2 and summarized in table 2.

6 Systematic uncertainty

The systematic uncertainties on the Born cross section measurement mainly originate from integrated luminosity, Ξ^- reconstruction, background, angular distribution, branching fraction, and input line shape. All of these sources of systematic uncertainty are discussed in detail below.
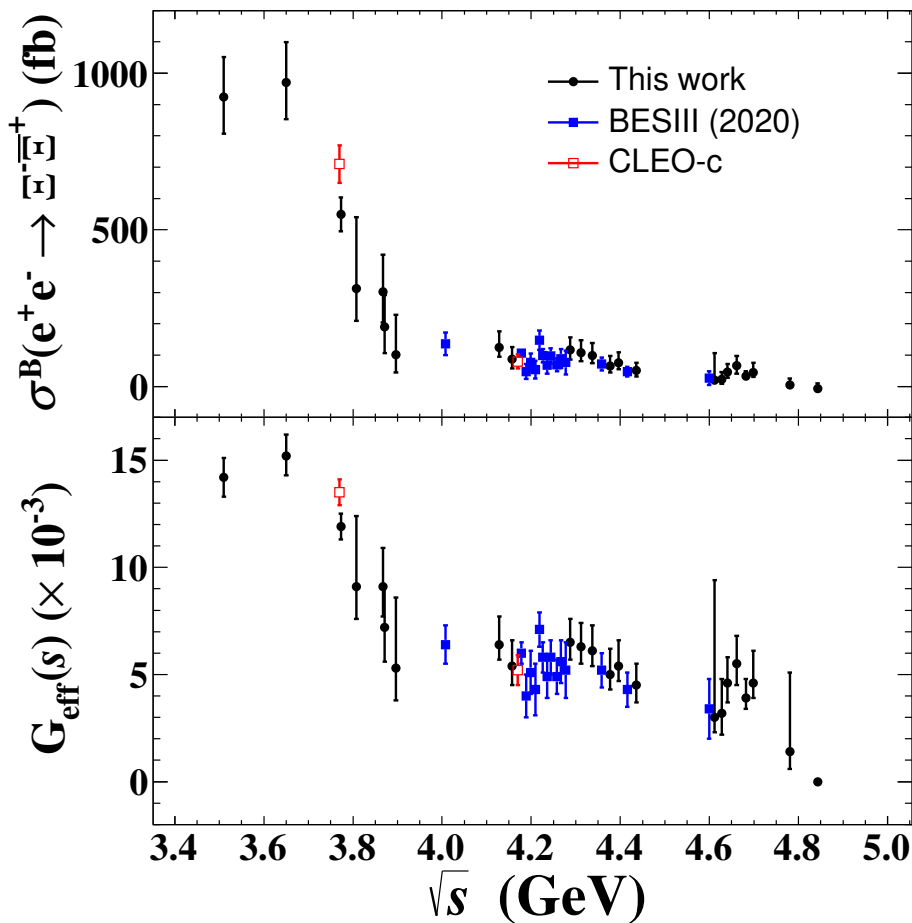
Figure 2. Measured Born cross section (top) and Ξ^- effective form factor (bottom) for $e^+e^- \to \Xi^-\bar{\Xi}^+$ as a function of the CM energy, where the uncertainties include both the statistical and systematic ones.

6.1 Luminosity

The integrated luminosity is measured using $e^+e^- \to (\gamma)e^+e^-$ events with a method similar to refs. [61–63] with an uncertainty of 1.0%.

6.2 Ξ^- reconstruction

The systematic uncertainty due to the Ξ^- reconstruction efficiency incorporating the tracking and PID efficiencies, the Λ reconstruction efficiency, the selection on Λ and Ξ^- decay lengths, and the Λ and Ξ^- mass windows, is estimated from a control sample of $\psi(3686) \to \Xi^-\bar{\Xi}^+$ decays with the same method as described in refs. [64–72]. The Ξ^- reconstruction efficiency is defined as the ratio of the number of events from the double baryon-tag $\Xi^-\bar{\Xi}^+$ to that from the single baryon-tag. The difference in the Ξ^- reconstruction efficiency between data and MC simulation is taken as the systematic uncertainty.

$\sqrt{s}$ (GeV)	$\mathcal{L}$ (pb^{-1})	$\frac{1}{\|1-\Pi\|^2}$	D ($\times 10^{-2}$)	N_{obs} (N^{UL})	σ^B (fb)	$\|G_{\text{eff}}(s)\|$ ($\times 10^{-3}$)	$\mathcal{S}$ (σ)
3.510	405.7	1.04	24.9 ± 0.1	$124.5^{+12.8}_{-11.1}$	$923.6^{+106.4}_{-92.3} \pm 70.2$	$14.2^{+0.8}_{-0.7} \pm 0.5$	10.4
3.650	410.0	1.02	25.6 ± 0.1	$132.5^{+12.8}_{-11.2}$	$970.8^{+105.1}_{-92.0} \pm 72.8$	$15.2^{+0.8}_{-0.7} \pm 0.6$	11.0
3.773	2931.8	1.06	27.7 ± 0.1	$602.2^{+27.7}_{-25.4}$	$548.8^{+28.4}_{-26.0} \pm 46.1$	$11.9^{+0.3}_{-0.3} \pm 0.5$	22.7
3.808	50.5	1.06	29.1 ± 0.2	$6.2^{+4.0}_{-1.7}$ (<13.2)	$312.2^{+225.6}_{-95.9} \pm 35.9$ (<664.7)	$9.1^{+3.3}_{-1.4} \pm 0.5$ (<13.3)	2.2
3.867	108.9	1.05	24.9 ± 0.1	$11.0^{+3.8}_{-3.1}$	$302.1^{+116.9}_{-95.4} \pm 22.7$	$9.1^{+1.8}_{-1.4} \pm 0.3$	3.2
3.871	110.3	1.05	24.9 ± 0.1	$7.0^{+3.3}_{-2.7}$ (<13.4)	$190.3^{+100.5}_{-82.2} \pm 14.3$ (<364.4)	$7.2^{+1.9}_{-1.6} \pm 0.3$ (<10.0)	2.3
3.896	52.6	1.05	25.1 ± 0.1	$1.8^{+2.0}_{-0.9}$ (<5.4)	$101.9^{+126.7}_{-57.0} \pm 7.6$ (<305.6)	$5.3^{+3.3}_{-1.5} \pm 0.2$ (<9.3)	1.2
4.128	401.5	1.05	22.6 ± 0.1	$15.2^{+5.4}_{-3.1}$	$124.9^{+49.7}_{-28.5} \pm 9.4$	$6.4^{+1.3}_{-0.7} \pm 0.2$	3.6
4.157	408.7	1.05	22.6 ± 0.1	$10.8^{+4.3}_{-3.2}$ (<18.8)	$86.9^{+38.7}_{-28.8} \pm 6.5$ (<151.2)	$5.4^{+1.2}_{-0.9} \pm 0.2$ (<7.1)	2.9
4.288	502.4	1.05	21.2 ± 0.1	$16.8^{+4.9}_{-3.8}$	$117.3^{+38.3}_{-29.7} \pm 8.8$	$6.5^{+1.1}_{-0.8} \pm 0.2$	3.8
4.312	501.2	1.05	21.3 ± 0.1	$15.5^{+5.0}_{-3.3}$	$107.9^{+39.0}_{-25.8} \pm 8.1$	$6.3^{+1.1}_{-0.8} \pm 0.2$	3.8
4.337	505.0	1.05	21.3 ± 0.1	$14.2^{+5.1}_{-2.9}$	$98.6^{+39.7}_{-22.6} \pm 7.4$	$6.1^{+1.2}_{-0.7} \pm 0.2$	3.6
4.377	522.7	1.05	20.9 ± 0.1	$9.5^{+4.2}_{-2.5}$ (<16.8)	$64.8^{+32.1}_{-19.1} \pm 4.9$ (<114.5)	$5.0^{+1.2}_{-0.7} \pm 0.2$ (<6.6)	2.9
4.396	507.8	1.05	20.5 ± 0.1	$10.5^{+4.2}_{-2.5}$	$75.2^{+33.7}_{-20.1} \pm 5.6$	$5.4^{+1.2}_{-0.7} \pm 0.2$	3.2
4.436	569.9	1.05	20.5 ± 0.2	$8.0^{+3.3}_{-2.7}$ (<14.3)	$51.0^{+23.6}_{-19.3} \pm 3.8$ (<91.2)	$4.5^{+1.0}_{-0.8} \pm 0.2$ (<6.0)	2.7
4.612	103.8	1.05	17.7 ± 0.2	$0.5^{+1.9}_{-0.2}$ (<3.7)	$20.2^{+86.1}_{-9.1} \pm 1.5$ (<149.6)	$3.0^{+6.4}_{-0.7} \pm 0.1$ (<8.1)	0.5
4.628	521.5	1.05	17.4 ± 0.2	$2.8^{+2.5}_{-1.5}$ (<7.5)	$22.9^{+22.9}_{-13.8} \pm 1.7$ (<61.5)	$3.2^{+1.6}_{-1.0} \pm 0.1$ (<5.2)	1.4
4.641	552.4	1.05	17.3 ± 0.1	$6.0^{+2.8}_{-2.1}$ (<11.1)	$46.5^{+24.3}_{-18.2} \pm 3.5$ (<86.1)	$4.6^{+1.2}_{-0.9} \pm 0.2$ (<6.2)	2.4
4.661	529.6	1.05	17.0 ± 0.1	$8.0^{+3.3}_{-2.7}$ (<14.3)	$66.2^{+30.6}_{-25.0} \pm 5.0$ (<118.3)	$5.5^{+1.3}_{-1.0} \pm 0.2$ (<7.3)	2.7
4.682	1669.3	1.05	16.7 ± 0.1	$12.2^{+5.1}_{-2.9}$	$32.5^{+15.2}_{-8.7} \pm 2.4$	$3.9^{+0.9}_{-0.5} \pm 0.1$	3.1
4.699	536.5	1.05	16.8 ± 0.1	$5.5^{+3.3}_{-1.6}$ (<11.1)	$45.2^{+30.4}_{-14.7} \pm 3.4$ (<91.3)	$4.6^{+1.5}_{-0.7} \pm 0.2$ (<6.5)	2.2
4.781	512.8	1.06	17.3 ± 0.2	$0.5^{+2.3}_{-0.5}$ (<4.6)	$4.2^{+21.5}_{-4.7} \pm 0.3$ (<38.5)	$1.4^{+3.7}_{-0.8} \pm 0.1$ (<4.3)	0.4
4.843	527.3	1.06	16.5 ± 0.2	$-0.8^{+1.7}_{-0.8}$ (<2.0)	$-6.8^{+16.2}_{-7.6} \pm 0.5$ (<17.0)	$0.0^{+0.0}_{-0.0} \pm 0.0$ (<2.9)	0.0

Table 2. The CM energy ($\sqrt{s}$), the integrated luminosity ($\mathcal{L}$), the VP correction factor ($\frac{1}{\|1-\Pi\|^2}$), the ISR correction factor and the detection efficiency ($D = (1+\delta)\epsilon$), the signal yields (N_{obs}), the upper limit of signal yield at the 90% confidence level (N^{UL}), the Born cross section (σ^B), the effective form factor ($\|G_{\text{eff}}(s)\|$) and the statistical significance ($\mathcal{S}$). The first and second uncertainties for σ^B are statistical and systematic, respectively.

6.3 Background

The systematic uncertainty associated with the background, which is estimated based on the sideband strategy, is determined by changing the gap between the signal region and the sideband regions from half box size to the full box size. Since the statistics for each energy points are very limited. To avoid the statistical effect, all energy points are combined when we estimate this systematic uncertainty. The difference of signal yields before and after changing the gap of the sideband box is taken as the systematic uncertainty.

6.4 Angular distribution

In this analysis, not enough statistics is available to determine the angular distribution parameter for each energy point separately. Thus, the selection efficiency for $e^+e^- \to \Xi^-\bar{\Xi}^+$ is determined based on a PHSP model, which may differ from the real angular distribution. Alternatively, we utilize the joint angular distribution obtained from ref. [71] to reproduce a MC sample, and take the efficiency difference between the signal MC samples and the alternative MC as the systematic uncertainty due to the angular distribution.

6.5 Branching fraction

The uncertainty from the branching fraction of $\Lambda \to p\pi^-$ is 0.8%, taken from the world average [49]. The uncertainty of the branching fraction of $\Xi^- \to \pi^- \Lambda$ is negligible.

6.6 Input line shape

The ISR correction and the detection efficiency depend on the input line shape of the cross section. The associated systematic uncertainty can be divided into two parts. One part is due to the statistical uncertainty of the input line shape of the cross section, which is estimated by varying the central value of the nominal input line shape within $\pm 1\sigma$ of statistical uncertainty. Then, the $(1 + \delta)\epsilon$ values for each energy point are recalculated. This process is repeated 3000 times, after which a Gaussian function is used to fit the $(1 + \delta)\epsilon$ distribution. The width of the Gaussian function is taken as the corresponding systematic uncertainty. The other uncertainty arises due to the resonance parameters which are fixed in the fit to the input cross section. The resonance parameters are changed in the fit by $\pm 1\sigma$ and the resulting changes of the values of $(1 + \delta)\epsilon$ are taken as the systematic uncertainty. The total systematic uncertainty is calculated by adding the two uncertainties in quadrature.

6.7 Total systematic uncertainty

The various systematic uncertainties on the Born cross section measurement are summarized in table 3. Assuming all sources are independent, the total systematic uncertainty on the cross section measurement is determined by adding these sources in quadrature.

7 Fit to the dressed cross section

Potential resonances in the line shape of the cross section for the reaction $e^+e^- \to \Xi^-\bar{\Xi}^+$ are studied by applying a fit to the dressed cross section, $\sigma^{\text{dressed}} = \sigma^B/|1 - \Pi|^2$ (without the VP effect) with the least square method. The fit minimizes

$$\chi^2 = \Delta X^T V^{-1} \Delta X, \tag{7.1}$$

where ΔX is the vector of residuals between measured and fitted cross section. The covariance matrix V incorporates the correlated and uncorrelated uncertainties among different energy points, where the systematic uncertainties due to the luminosity, Ξ^- reconstruction and branching fraction are assumed to be fully correlated among CM energies and the other ones are uncorrelated.

Assuming the cross section of $e^+e^- \to \Xi^-\bar{\Xi}^+$ includes a resonance plus a continuum contribution, a fit to the dressed cross section with the coherent sum of a power-law (PL) function and a Breit-Wigner (BW) function

$$\sigma^{\text{dressed}}\left(\sqrt{s}\right) = \left| c_0 \frac{\sqrt{P\left(\sqrt{s}\right)}}{\sqrt{s}^n} + e^{i\phi}\text{BW}\left(\sqrt{s}\right)\sqrt{\frac{P\left(\sqrt{s}\right)}{P(M)}} \right|^2, \tag{7.2}$$

$\sqrt{s}$ (GeV)	Luminosity	Ξ^- reconstruction	Background	AD	$\mathcal{B}$	ILS	Total
3.510						1.2	7.6
3.650						1.1	7.5
3.773						3.8	8.4
3.808						8.7	11.5
3.867						0.9	7.5
3.871						1.1	7.5
3.896						0.8	7.5
4.128						0.6	7.5
4.157						0.4	7.5
4.288						1.1	7.5
4.312						0.6	7.5
4.337	1.0	5.7	1.7	4.3	0.8	0.2	7.5
4.377						0.5	7.5
4.396						0.5	7.5
4.436						1.0	7.5
4.612						1.3	7.6
4.628						1.0	7.5
4.641						0.3	7.5
4.661						0.4	7.5
4.682						0.1	7.5
4.699						1.5	7.6
4.781						0.6	7.5
4.843						2.2	7.8

Table 3. Systematic uncertainties (in %) and their sources for each energy point on the Born cross section measurement. Here, AD denotes angular distribution, $\mathcal{B}$ denotes branching fraction, and ILS denotes input line shape. The systematic uncertainty, which is the same for each energy point, is simplified into a single numerical value.

is applied. Here ϕ is the relative phase between the BW function

$$\text{BW}\left(\sqrt{s}\right) = \frac{\sqrt{12\pi\Gamma_{ee}\mathcal{B}\Gamma}}{s - M^2 + iM\Gamma},\tag{7.3}$$

and the PL function, c_0 and n are free fit parameters, $\sqrt{P(\sqrt{s})}$ is the two-body phase space factor, the mass M and total width Γ are fixed to the assumed resonance with the PDG values [49], and $\Gamma_{ee}\mathcal{B}$ is the product of the electronic partial width and the branching fraction for the assumed resonance decaying into the $\Xi^-\bar{\Xi}^+$ final state. A fit without resonance contribution results in parameters ($c_0 = 1.8 \pm 0.4, n = 8.2 \pm 0.2$) with the goodness of fit $\chi^2/n.d.f = 75.5/(38 - 2)$. The result of the fit with $\psi(3770)$ plus a continuum contribution is presented in table 4. Due to ambiguities in the fit, multiple solutions with the same likelihood are found [73]. Both solutions are presented in table 4 under the inclusion of different resonant states. The result of the fit with the $\psi(3770)$ plus

a continuum contribution is presented in table 4. Since the two solutions of this fit are very close, only a single solution is considered. When the other possible charmonium(- like) states, $\psi(4040)$, $\psi(4160)$, $Y(4230)$, $Y(4360)$, $\psi(4415)$, $Y(4660)$ are included one-by-one in the fit, in addition to the $\psi(3770)$ plus continuum, the result of the $\psi(3770)$ is nearly unchanged. Therefore, only the results corresponding to the additional charmonium(-like) states are presented in table 4. Taking systematic uncertainties into account, the significance of the resonance contribution is calculated by comparing $\chi^2/n.d.f$ with and without the resonance assumption. For different assumptions, n is almost unchanged. Evidence for the decay $\psi(3770) \to \Xi^- \bar{\Xi}^+$ with a significance of 4.5σ including the systematic uncertainty is found by combining these results with earlier BESIII measurements [26]. For other possible charmonium(-like) states, no obvious signal is found and the upper limits on the products of branching fraction and two-electronic partial width for these charmonium(-like) states decaying into the $\Xi^- \bar{\Xi}^+$ final state including the systematic uncertainty are provided at the 90% confidence level (C.L.) using a Bayesian approach [74]. Systematic uncertainties due to beam energy, mass, and width of the $\psi(3770)$ resonance have been considered by varying the known values within one standard deviation; they turn out to be negligible. Figure 3 shows the fit to the dressed cross section with and without assumption of resonance contributions.

8 Summary

Using a total of $12.9\,\mathrm{fb}^{-1}$ of e^+e^- collision data above the open-charm threshold collected with the BESIII detector at the BEPCII collider, the process $e^+e^- \to \Xi^- \bar{\Xi}^+$ is studied based on a single baryon-tag technique. The Born cross sections and effective form factors are measured at 23 CM energies in the range from 3.510 to 4.843 GeV. Combined with earlier BESIII measurements [26], a fit to the dressed cross section of the reaction $e^+e^- \to \Xi^- \bar{\Xi}^+$ is performed, in which the line shape is described by a $\psi(3770)$ plus a continuum contribution. First evidence for the decay $\psi(3770) \to \Xi^- \bar{\Xi}^+$ is found with a significance of 4.5σ, accounting also for the systematic uncertainty. The branching fraction is determined to be $\mathcal{B}(\psi(3770) \to \Xi^- \bar{\Xi}^+) = (136.0 \pm 35.2) \times 10^{-6}$, which is larger by at least an order of magnitude than the prediction (4×10^{-7}) based on a scaling from the electronic branching fraction values using eq. (1) in ref. [54]. This implies that the $\psi(3770)$ resonance needs to be considered when interpreting the CLEO-c data. No obvious signal from $\psi(4040)$, $\psi(4160)$, $Y(4230)$, $Y(4360)$, $\psi(4415)$, or $Y(4660)$ has been found. Thus, the upper limits of the products of branching fraction and electronic partial width for these charmonium(-like) states decaying into the $\Xi^- \bar{\Xi}^+$ final state are provided at the 90% C.L. This measurement provides evidence of non-$D\bar{D}$ decays of $\psi(3770)$, and can be useful for the understanding of the charmonium(-like) states coupling to the baryon-antibaryon final states. It gives additional insight into the puzzle of a large non-$D\bar{D}$ component of $\psi(3770)$ state.
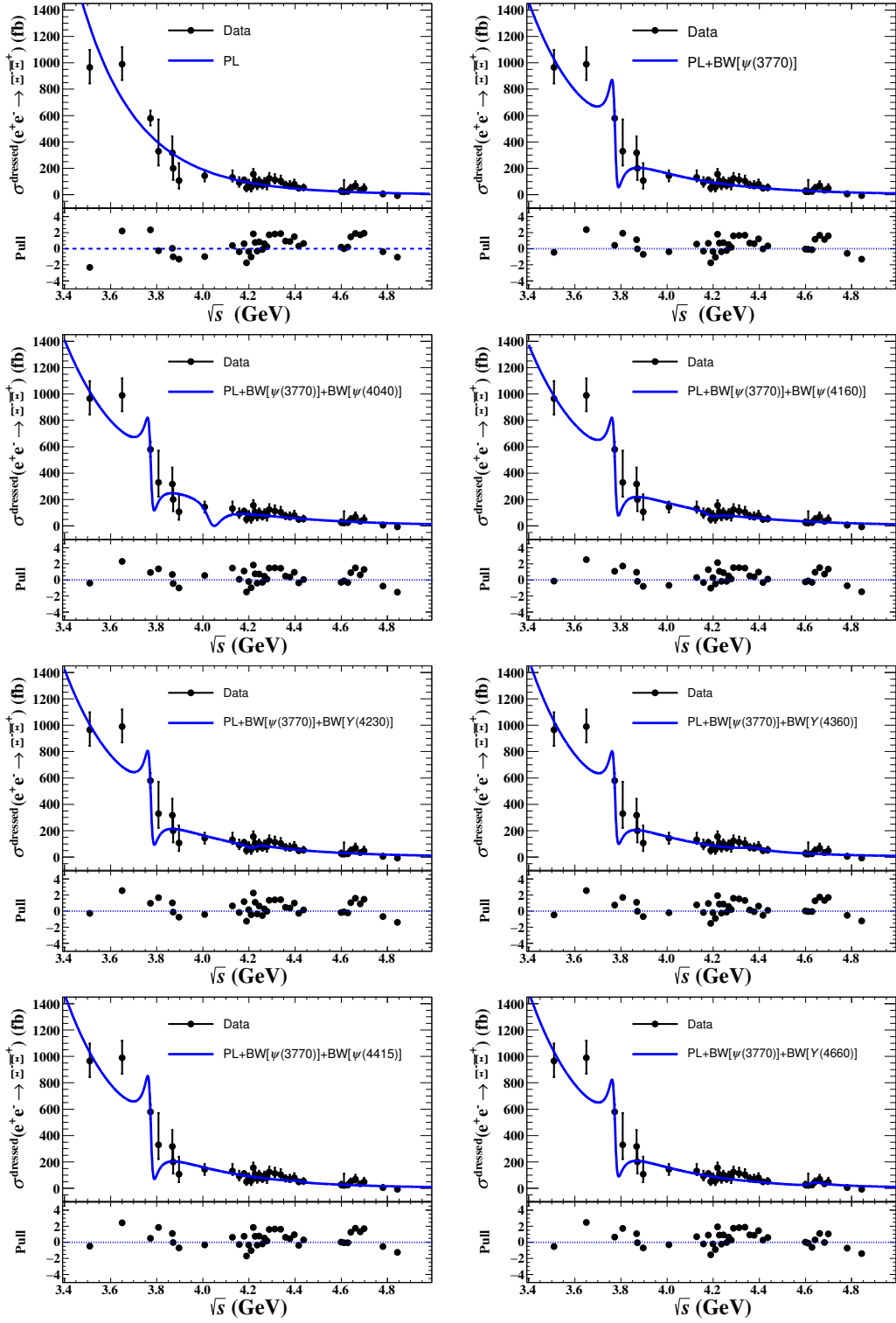
Figure 3. Fits to the dressed cross section at the CM energy from 3.510 to 4.843 GeV with the assumptions of a PL function only (first one), a PL function plus a ($\psi(3770)$) resonance, a PL function plus a ($\psi(3770)$) resonance and one more additional resonance ($\psi(4040)$, $\psi(4160)$, $Y(4230)$, $Y(4360)$, $\psi(4415)$, and $Y(4660)$). Dots with error bars are the dressed cross sections and the solid lines show the fit results.

Resonance parameter	Solution I	Solution II	$\chi^2/n.d.f$
$\phi_{\psi(3770)}$ (rad)	-2.1 ± 0.2	$-$	
$\Gamma_{ee}\mathcal{B}_{\psi(3770)}$ $(10^{-3}\,\mathrm{eV})$	35.5 ± 9.2	$-$	$45.0/(38-4)$
$\mathcal{B}[\psi(3770) \to \Xi^-\bar{\Xi}^+]$ (10^{-6})	136.0 ± 35.2	$-$	
$\phi_{\psi(4040)}$ (rad)	-1.9 ± 0.2	-2.5 ± 0.1	
$\Gamma_{ee}\mathcal{B}_{\psi(4040)}$ $(10^{-3}\,\mathrm{eV})$	15.2 ± 27.6 (< 44.0)	19.7 ± 30.9 (< 51.9)	$37.1/(38-6)$
$\mathcal{B}[\psi(4040) \to \Xi^-\bar{\Xi}^+]$ (10^{-6})	17.8 ± 32.2 (< 51.4)	23.0 ± 36.1 (< 60.6)	
$\phi_{\psi(4160)}$ (rad)	-1.7 ± 0.1	-2.3 ± 0.1	
$\Gamma_{ee}\mathcal{B}_{\psi(4160)}$ $(10^{-3}\,\mathrm{eV})$	29.8 ± 2.5 (< 32.9)	33.9 ± 2.7 (< 37.2)	$38.1/(38-6)$
$\mathcal{B}[\psi(4160) \to \Xi^-\bar{\Xi}^+]$ (10^{-6})	61.7 ± 5.2 (< 68.1)	70.2 ± 5.6 (< 77.0)	
$\phi_{Y(4230)}$ (rad)	-1.7 ± 0.1	-2.2 ± 0.1	
$\Gamma_{ee}\mathcal{B}_{Y(4230)}$ $(10^{-3}\,\mathrm{eV})$	19.4 ± 1.9 (< 22.3)	22.0 ± 2.1 (< 25.1)	$39.5/(38-6)$
$\mathcal{B}[Y(4230) \to \Xi^-\bar{\Xi}^+]$ (10^{-6})	$-$	$-$	
$\phi_{Y(4360)}$ (rad)	-1.8 ± 0.1	-2.1 ± 0.1	
$\Gamma_{ee}\mathcal{B}_{Y(4360)}$ $(10^{-3}\,\mathrm{eV})$	36.0 ± 3.2 (< 41.2)	39.4 ± 3.3 (< 44.8)	$41.7/(38-6)$
$\mathcal{B}[Y(4360) \to \Xi^-\bar{\Xi}^+]$ (10^{-6})	$-$	$-$	
$\phi_{\psi(4415)}$ (rad)	-1.7 ± 0.1	-2.2 ± 0.1	
$\Gamma_{ee}\mathcal{B}_{\psi(4415)}$ $(10^{-3}\,\mathrm{eV})$	16.5 ± 1.9 (< 19.8)	18.3 ± 2.0 (< 21.7)	$44.5/(38-6)$
$\mathcal{B}[\psi(4415) \to \Xi^-\bar{\Xi}^+]$ (10^{-6})	28.3 ± 3.3 (< 34.0)	31.4 ± 3.4 (< 37.2)	
$\phi_{Y(4660)}$ (rad)	-1.6 ± 0.1	-2.2 ± 0.1	
$\Gamma_{ee}\mathcal{B}_{Y(4660)}$ $(10^{-3}\,\mathrm{eV})$	13.6 ± 2.0 (< 18.0)	15.3 ± 2.2 (< 19.9)	$41.1/(38-6)$
$\mathcal{B}[Y(4660) \to \Xi^-\bar{\Xi}^+]$ (10^{-6})	$-$	$-$	

Table 4. The fitted resonance parameters to the dressed cross section for the $e^+e^- \to \Xi^-\bar{\Xi}^+$ process for the two ambiguous solutions. The fit procedure includes both statistical and systematic uncertainties except for the CM energy calibration. The top row represents the result for $\psi(3770)$ plus a continuum. Only one solution is found in this case. The other rows represent the results of the resonances $\psi(4040)$, $\psi(4160)$, $Y(4230)$, $Y(4360)$, $\psi(4415)$, and $Y(4660)$, respectively, when they are added one-by-one to the fit in addition to the $\psi(3770)$ plus a continuum. The $\mathcal{B}$ is the branching fraction for the assumed resonance decaying into $\Xi^-\bar{\Xi}^+$ final state, where possible, $\mathcal{B}$ is determined using Γ_{ee} values from PDG [49].

Acknowledgments

References

[1] T. Barnes, S. Godfrey and E.S. Swanson, *Higher charmonia*, *Phys. Rev. D* **72** (2005) 054026 [`hep-ph/0505002`] [ɪɴSPIRE].

[2] BES collaboration, *Measurements of the cross section for $e^+e^- \rightarrow hadrons$ at center-of-mass energies from 2 GeV to 5 GeV*, *Phys. Rev. Lett.* **88** (2002) 101802 [`hep-ex/0102003`] [ɪɴSPIRE].

[3] BaBar collaboration, *Observation of a broad structure in the $\pi^+\pi^- J/\psi$ mass spectrum around 4.26 GeV/c^2*, *Phys. Rev. Lett.* **95** (2005) 142001 [`hep-ex/0506081`] [ɪɴSPIRE].

[4] BaBar collaboration, *Evidence of a broad structure at an invariant mass of 4.32 GeV/c^2 in the reaction $e^+e^- \rightarrow \pi^+\pi^-\psi(2S)$ measured at BaBar*, *Phys. Rev. Lett.* **98** (2007) 212001 [`hep-ex/0610057`] [ɪɴSPIRE].

[5] Belle collaboration, *Observation of Two Resonant Structures in $e^+e^- \rightarrow \pi^+\pi^-\psi(2S)$ via Initial State Radiation at Belle*, *Phys. Rev. Lett.* **99** (2007) 142002 [`arXiv:0707.3699`] [ɪɴSPIRE].

[6] Belle collaboration, *Measurement of $e^+e^- \rightarrow \pi^+\pi^- J/\psi$ cross section via initial state radiation at Belle*, *Phys. Rev. Lett.* **99** (2007) 182004 [`arXiv:0707.2541`] [ɪɴSPIRE].

[7] Belle collaboration, *Observation of a near-threshold enhancement in the $e^+e^- \rightarrow \Lambda_c^+\bar{\Lambda}_c^-$ cross section using initial-state radiation*, *Phys. Rev. Lett.* **101** (2008) 172001 [`arXiv:0807.4458`] [ɪɴSPIRE].

[8] BaBar collaboration, *Study of the reaction $e^+e^- \rightarrow J/\psi\pi^+\pi^-$ via initial-state radiation at BaBar*, *Phys. Rev. D* **86** (2012) 051102 [`arXiv:1204.2158`] [ɪɴSPIRE].

[9] Belle collaboration, *Study of $e^+e^- \rightarrow \pi^+\pi^- J/\psi$ and Observation of a Charged Charmoniumlike State at Belle*, *Phys. Rev. Lett.* **110** (2013) 252002 [*Erratum ibid.* **111** (2013) 019901] [`arXiv:1304.0121`] [ɪɴSPIRE].

[10] BaBar collaboration, *Study of the reaction $e^+e^- \to \psi(2S)\pi^+\pi^-$ via initial-state radiation at BaBar*, *Phys. Rev. D* **89** (2014) 111103 [arXiv:1211.6271] [InSPIRE].

[11] Belle collaboration, *Measurement of $e^+e^- \to \pi^+\pi^-\psi(2S)$ via Initial State Radiation at Belle*, *Phys. Rev. D* **91** (2015) 112007 [arXiv:1410.7641] [InSPIRE].

[12] CLEO collaboration, *Charmonium decays of $Y(4260)$, $\psi(4160)$ and $\psi(4040)$*, *Phys. Rev. Lett.* **96** (2006) 162003 [hep-ex/0602034] [InSPIRE].

[13] BESIII collaboration, *Study of $e^+e^- \to \omega\chi_{cJ}$ at center-of-mass energies from 4.21 to 4.42 GeV*, *Phys. Rev. Lett.* **114** (2015) 092003 [arXiv:1410.6538] [InSPIRE].

[14] BESIII collaboration, *Observation of Three Charmoniumlike States with $J^{PC} = 1^{--}$ in $e^+e^- \to D^{*0}D^{*-}\pi^+$*, *Phys. Rev. Lett.* **130** (2023) 121901 [arXiv:2301.07321] [InSPIRE].

[15] F.E. Close and P.R. Page, *Gluonic charmonium resonances at BaBar and BELLE*, *Phys. Lett. B* **628** (2005) 215 [hep-ph/0507199] [InSPIRE].

[16] N. Brambilla et al., *Heavy Quarkonium: Progress, Puzzles, and Opportunities*, *Eur. Phys. J. C* **71** (2011) 1534 [arXiv:1010.5827] [InSPIRE].

[17] R.A. Briceno et al., *Issues and Opportunities in Exotic Hadrons*, *Chin. Phys. C* **40** (2016) 042001 [arXiv:1511.06779] [InSPIRE].

[18] L.-G. Xia, *Study of $\psi(3770)$ decaying to baryon anti-baryon pairs*, *Phys. Lett. B* **756** (2016) 77 [arXiv:1508.02039] [InSPIRE].

[19] H.-X. Chen, W. Chen, X. Liu and S.-L. Zhu, *The hidden-charm pentaquark and tetraquark states*, *Phys. Rept.* **639** (2016) 1 [arXiv:1601.02092] [InSPIRE].

[20] R.-Q. Qian, Q. Huang and X. Liu, *Predicted $\Lambda\bar{\Lambda}$ and $\Xi^-\bar{\Xi}^+$ decay modes of the charmoniumlike $Y(4230)$*, *Phys. Lett. B* **833** (2022) 137292 [arXiv:2111.13821] [InSPIRE].

[21] Z.-Y. Bai, Q.-S. Zhou and X. Liu, *Higher strangeonium decays into a light flavor baryon pair like $\Lambda\bar{\Lambda}$, $\Sigma\bar{\Sigma}$, and $\Xi\bar{\Xi}$*, arXiv:2307.16255 [InSPIRE].

[22] B. Yan, C. Chen and J.-J. Xie, *Σ and Ξ electromagnetic form factors in the extended vector meson dominance model*, *Phys. Rev. D* **107** (2023) 076008 [arXiv:2301.00976] [InSPIRE].

[23] J.-P. Dai, X. Cao and H. Lenske, *Data driven isospin analysis of timelike octet baryons electromagnetic form factors and charmonium decay into baryon-anti-baryon*, *Phys. Lett. B* **846** (2023) 138192 [arXiv:2304.04913] [InSPIRE].

[24] BESIII collaboration, *Search for Baryonic Decays of $\psi(3770)$ and $\psi(4040)$*, *Phys. Rev. D* **87** (2013) 112011 [arXiv:1305.1782] [InSPIRE].

[25] BESIII collaboration, *Precision measurement of the $e^+e^- \to \Lambda_c^+\bar{\Lambda}_c^-$ cross section near threshold*, *Phys. Rev. Lett.* **120** (2018) 132001 [arXiv:1710.00150] [InSPIRE].

[26] BESIII collaboration, *Measurement of the Cross Section for $e^+e^- \to \Xi^-\bar{\Xi}^+$ and Observation of an Excited Ξ Baryon*, *Phys. Rev. Lett.* **124** (2020) 032002 [arXiv:1910.04921] [InSPIRE].

[27] H. Liu, J. Zhang and X. Wang, *CP Asymmetry in the Ξ Hyperon Sector*, *Symmetry* **15** (2023) 214 [InSPIRE].

[28] BESIII collaboration, *Study of baryon pair production at BESIII*, *PoS* **CHARM2020** (2021) 026 [InSPIRE].

[29] BESIII collaboration, *Measurement of the cross section for $e^+e^- \to \Lambda\bar{\Lambda}$ and evidence of the decay $\psi(3770) \to \Lambda\bar{\Lambda}$*, *Phys. Rev. D* **104** (2021) L091104 [arXiv:2108.02410] [InSPIRE].

[30] X. Wang, *Hyperon pair production at BESIII*, *Rev. Mex. Fis. Suppl.* **3** (2022) 0308074 [ɪɴSPIRE].

[31] BESIII collaboration, *Design and Construction of the BESIII Detector*, *Nucl. Instrum. Meth. A* **614** (2010) 345 [`arXiv:0911.4960`] [ɪɴSPIRE].

[32] C. Yu et al., *BEPCII Performance and Beam Dynamics Studies on Luminosity*, in the proceedings of the *7th International Particle Accelerator Conference*, Busan, Korea, Republic of, May 08–13 (2016), p. TUYA01 [`DOI:10.18429/JACoW-IPAC2016-TUYA01`] [ɪɴSPIRE].

[33] BESIII collaboration, *Future Physics Programme of BESIII*, *Chin. Phys. C* **44** (2020) 040001 [`arXiv:1912.05983`] [ɪɴSPIRE].

[34] J. Lu, Y. Xiao and X. Ji, *Online monitoring of the center-of-mass energy from real data at BESIII*, *Radiat. Detect. Technol. Methods* **4** (2020) 337.

[35] J.-W. Zhang et al., *Suppression of top-up injection backgrounds with offline event filter in the BESIII experiment*, *Radiat. Detect. Technol. Methods* **6** (2022) 289 [ɪɴSPIRE].

[36] X. Li et al., *Study of MRPC technology for BESIII endcap-TOF upgrade*, *Radiat. Detect. Technol. Methods* **1** (2017) 13.

[37] Y.X. Guo et al., *The study of time calibration for upgraded end cap TOF of BESIII*, *Radiat. Detect. Technol. Methods* **1** (2017) 15.

[38] P. Cao et al., *Design and construction of the new BESIII endcap Time-of-Flight system with MRPC Technology*, *Nucl. Instrum. Meth. A* **953** (2020) 163053 [ɪɴSPIRE].

[39] GEANT4 collaboration, *GEANT4 — a simulation toolkit*, *Nucl. Instrum. Meth. A* **506** (2003) 250 [ɪɴSPIRE].

[40] K.-X. Huang et al., *Method for detector description transformation to Unity and application in BESIII*, *Nucl. Sci. Tech.* **33** (2022) 142 [`arXiv:2206.10117`] [ɪɴSPIRE].

[41] D.J. Lange, *The EvtGen particle decay simulation package*, *Nucl. Instrum. Meth. A* **462** (2001) 152 [ɪɴSPIRE].

[42] R.-G. Ping, *Event generators at BESIII*, *Chin. Phys. C* **32** (2008) 599 [ɪɴSPIRE].

[43] S. Jadach, B.F.L. Ward and Z. Was, *Coherent exclusive exponentiation for precision Monte Carlo calculations*, *Phys. Rev. D* **63** (2001) 113009 [`hep-ph/0006359`] [ɪɴSPIRE].

[44] BESIII collaboration, *Measurements of baryon pair decays of χ_{cJ} mesons*, *Phys. Rev. D* **87** (2013) 032007 [*Erratum ibid.* **87** (2013) 059901] [`arXiv:1211.2283`] [ɪɴSPIRE].

[45] BESIII collaboration, *Measurement of Λ baryon polarization in $e^+e^- \to \Lambda\bar{\Lambda}$ at $\sqrt{s} = 3.773\,GeV$*, *Phys. Rev. D* **105** (2022) L011101 [`arXiv:2111.11742`] [ɪɴSPIRE].

[46] BESIII collaboration, *Measurement of Λ transverse polarization in e^+e^- collisions at $\sqrt{s} = 3.68 - 3.71\,GeV$*, *JHEP* **10** (2023) 081 [`arXiv:2303.00271`] [ɪɴSPIRE].

[47] BESIII collaboration, *Study of $e^+e^- \to \Omega^-\bar{\Omega}^+$ at center-of-mass energies from 3.49 to 3.67 GeV*, *Phys. Rev. D* **107** (2023) 052003 [`arXiv:2212.03693`] [ɪɴSPIRE].

[48] M. Xu et al., *Decay vertex reconstruction and 3-dimensional lifetime determination at BESIII*, *Chin. Phys. C* **33** (2009) 428 [ɪɴSPIRE].

[49] PARTICLE DATA GROUP collaboration, *Review of Particle Physics*, *PTEP* **2022** (2022) 083C01 [ɪɴSPIRE].

[50] J. Lundberg, J. Conrad, W. Rolke and A. Lopez, *Limits, discovery and cut optimization for a Poisson process with uncertainty in background and signal efficiency: TRolke 2.0*, *Comput. Phys. Commun.* **181** (2010) 683 [arXiv:0907.3450] [INSPIRE].

[51] E.A. Kuraev and V.S. Fadin, *On Radiative Corrections to e^+e^- Single Photon Annihilation at High-Energy*, *Sov. J. Nucl. Phys.* **41** (1985) 466 [INSPIRE].

[52] F. Jegerlehner and R. Szafron, *$\rho^0 - \gamma$ mixing in the neutral channel pion form factor F_π^e and its role in comparing e^+e^- with τ spectral functions*, *Eur. Phys. J. C* **71** (2011) 1632 [arXiv:1101.2872] [INSPIRE].

[53] W. Sun et al., *An iterative weighting method to apply ISR correction to e^+e^- hadronic cross section measurements*, *Front. Phys. (Beijing)* **16** (2021) 64501 [arXiv:2011.07889] [INSPIRE].

[54] S. Dobbs et al., *Hyperon Form Factors & Diquark Correlations*, *Phys. Rev. D* **96** (2017) 092004 [arXiv:1708.09377] [INSPIRE].

[55] R. Baldini, S. Pacetti, A. Zallo and A. Zichichi, *Unexpected features of $e^+e^- \to p\bar{p}$ and $e^+e^- \to \Lambda\bar{\Lambda}$ cross sections near threshold*, *Eur. Phys. J. A* **39** (2009) 315 [arXiv:0711.1725] [INSPIRE].

[56] A.B. Arbuzov and T.V. Kopylova, *On relativization of the Sommerfeld-Gamow-Sakharov factor*, *JHEP* **04** (2012) 009 [arXiv:1111.4308] [INSPIRE].

[57] A. Sommerfeld, *Über die Beugung und Bremsung der Elektronen*, *Annalen Phys.* **403** (1931) 257 [INSPIRE].

[58] C. Tzara, *Effect of the coulomb potential on the $\pi-$ photoproduction*, *Nucl. Phys. B* **18** (1970) 246 [INSPIRE].

[59] A.D. Sakharov, *Interaction of the electron and the positron in pair production*, *Zh. Eksp. Teor. Fiz.* **18** (1948) 631 [INSPIRE].

[60] X. Wang and G. Huang, *Electromagnetic Form Factor of Doubly-Strange Hyperon*, *Symmetry* **14** (2022) 65 [INSPIRE].

[61] BESIII collaboration, *Precision measurement of the integrated luminosity of the data taken by BESIII at center of mass energies between 3.810 GeV and 4.600 GeV*, *Chin. Phys. C* **39** (2015) 093001 [arXiv:1503.03408] [INSPIRE].

[62] BESIII collaboration, *Measurement of integrated luminosities at BESIII for data samples at center-of-mass energies between 4.0 and 4.6 GeV*, *Chin. Phys. C* **46** (2022) 113002 [arXiv:2203.03133] [INSPIRE].

[63] BESIII collaboration, *Luminosities and energies of e^+e^- collision data taken between 4.61 GeV and 4.95 GeV at BESIII*, *Chin. Phys. C* **46** (2022) 113003 [arXiv:2205.04809] [INSPIRE].

[64] BESIII collaboration, *Study of ψ decays to the $\Xi^-\bar{\Xi}^+$ and $\Sigma(1385)^\mp\bar{\Sigma}(1385)^\pm$ final states*, *Phys. Rev. D* **93** (2016) 072003 [arXiv:1602.06754] [INSPIRE].

[65] BESIII collaboration, *Study of J/ψ and $\psi(3686) \to \Sigma(1385)^0\bar{\Sigma}(1385)^0$ and $\Xi^0\bar{\Xi}^0$*, *Phys. Lett. B* **770** (2017) 217 [arXiv:1612.08664] [INSPIRE].

[66] BESIII collaboration, *Observation of $\psi(3686) \to \Xi(1530)^-\bar{\Xi}(1530)^+$ and $\Xi(1530)^-\bar{\Xi}^+$*, *Phys. Rev. D* **100** (2019) 051101 [arXiv:1907.13041] [INSPIRE].

[67] BESIII collaboration, *Measurement of cross section for $e^+e^- \to \Xi^-\bar{\Xi}^+$ near threshold at BESIII*, *Phys. Rev. D* **103** (2021) 012005 [arXiv:2010.08320] [INSPIRE].

[68] BESIII collaboration, *Measurement of cross section for $e^+e^- \to \Xi^0\bar{\Xi}^0$ near threshold*, *Phys. Lett. B* **820** (2021) 136557 [`arXiv:2105.14657`] [INSPIRE].

[69] BESIII collaboration, *Observation of $\psi(3686) \to \Xi(1530)^0\bar{\Xi}(1530)^0$ and $\Xi(1530)^0\bar{\Xi}^0$*, *Phys. Rev. D* **104** (2021) 092012 [`arXiv:2109.06621`] [INSPIRE].

[70] BESIII collaboration, *Study of the processes $\chi_{cJ} \to \Xi^-\bar{\Xi}^+$ and $\Xi^0\bar{\Xi}^0$*, *JHEP* **06** (2022) 074 [`arXiv:2202.08058`] [INSPIRE].

[71] BESIII collaboration, *Observation of Ξ^- hyperon transverse polarization in $\psi(3686) \to \Xi^-\bar{\Xi}^+$*, *Phys. Rev. D* **106** (2022) L091101 [`arXiv:2206.10900`] [INSPIRE].

[72] BESIII collaboration, *First Simultaneous Measurement of Ξ^0 and $\bar{\Xi}^0$ Asymmetry Parameters in $\psi(3686)$ Decay*, *Phys. Rev. D* **108** (2023) L011101 [`arXiv:2302.09767`] [INSPIRE].

[73] Y. Bai and D.-Y. Chen, *General mathematical analysis on multiple solutions of interfering resonances combinations*, *Phys. Rev. D* **99** (2019) 072007 [`arXiv:1901.01394`] [INSPIRE].

[74] Y.-S. Zhu, *Bayesian credible interval construction for Poisson statistics*, *Chin. Phys. C* **32** (2008) 363 [`arXiv:0812.2705`] [INSPIRE].

The BESIII collaboration

M. Ablikim[1], M.N. Achasov[5,b], P. Adlarson[74], X.C. Ai[80], R. Aliberti[35], A. Amoroso[73A,73C], M.R. An[39], Q. An[70,57], Y. Bai[56], O. Bakina[36], I. Balossino[29A], Y. Ban[46,g], V. Batozskaya[1,44], K. Begzsuren[32], N. Berger[35], M. Berlowski[44], M. Bertani[28A], D. Bettoni[29A], F. Bianchi[73A,73C], E. Bianco[73A,73C], A. Bortone[73A,73C], I. Boyko[36], R.A. Briere[6], A. Brueggemann[67], H. Cai[75], X. Cai[1,57], A. Calcaterra[28A], G.F. Cao[1,62], N. Cao[1,62], S.A. Cetin[61A], J.F. Chang[1,57], T.T. Chang[76], W.L. Chang[1,62], G.R. Che[43], G. Chelkov[36,a], C. Chen[43], Chao Chen[54], G. Chen[1], H.S. Chen[1,62], M.L. Chen[1,57,62], S.J. Chen[42], S.M. Chen[60], T. Chen[1,62], X.R. Chen[31,62], X.T. Chen[1,62], Y.B. Chen[1,57], Y.Q. Chen[34], Z.J. Chen[25,h], W.S. Cheng[73C], S.K. Choi[11], X. Chu[43], G. Cibinetto[29A], S.C. Coen[4], F. Cossio[73C], J.J. Cui[49], H.L. Dai[1,57], J.P. Dai[78], A. Dbeyssi[18], R. E. de Boer[4], D. Dedovich[36], Z.Y. Deng[1], A. Denig[35], I. Denysenko[36], M. Destefanis[73A,73C], F. De Mori[73A,73C], B. Ding[65,1], X.X. Ding[46,g], Y. Ding[40], Y. Ding[34], J. Dong[1,57], L.Y. Dong[1,62], M.Y. Dong[1,57,62], X. Dong[75], M.C. Du[1], S.X. Du[80], Z.H. Duan[42], P. Egorov[36,a], Y.H.Y. Fan[45], Y.L. Fan[75], J. Fang[1,57], S.S. Fang[1,62], W.X. Fang[1], Y. Fang[1], R. Farinelli[29A], L. Fava[73B,73C], F. Feldbauer[4], G. Felici[28A], C.Q. Feng[70,57], J.H. Feng[58], K Fischer[68], M. Fritsch[4], C. Fritzsch[67], C.D. Fu[1], J.L. Fu[62], Y.W. Fu[1], H. Gao[62], Y.N. Gao[46,g], Yang Gao[70,57], S. Garbolino[73C], I. Garzia[29A,29B], P.T. Ge[75], Z.W. Ge[42], C. Geng[58], E.M. Gersabeck[66], A Gilman[68], K. Goetzen[14], L. Gong[40], W.X. Gong[1,57], W. Gradl[35], S. Gramigna[29A,29B], M. Greco[73A,73C], M.H. Gu[1,57], C. Y Guan[1,62], Z.L. Guan[22], A.Q. Guo[31,62], L.B. Guo[41], M.J. Guo[49], R.P. Guo[48], Y.P. Guo[13,f], A. Guskov[36,a], T.T. Han[49], W.Y. Han[39], X.Q. Hao[19], F.A. Harris[64], K.K. He[54], K.L. He[1,62], F.H.H. Heinsius[4], C.H. Heinz[35], Y.K. Heng[1,57,62], C. Herold[59], T. Holtmann[4], P.C. Hong[13,f], G.Y. Hou[1,62], X.T. Hou[1,62], Y.R. Hou[62], Z.L. Hou[1], H.M. Hu[1,62], J.F. Hu[55,i], T. Hu[1,57,62], Y. Hu[1], G.S. Huang[70,57], K.X. Huang[58], L.Q. Huang[31,62], X.T. Huang[49], Y.P. Huang[1], T. Hussain[72], N Hüsken[27,35], W. Imoehl[27], J. Jackson[27], S. Jaeger[4], S. Janchiv[32], J.H. Jeong[11], Q. Ji[1], Q.P. Ji[19], X.B. Ji[1,62], X.L. Ji[1,57], Y.Y. Ji[49], X.Q. Jia[49], Z.K. Jia[70,57], H.J. Jiang[75], P.C. Jiang[46,g], S.S. Jiang[39], T.J. Jiang[16], X.S. Jiang[1,57,62], Y. Jiang[62], J.B. Jiao[49], Z. Jiao[23], S. Jin[42], Y. Jin[65], M.Q. Jing[1,62], T. Johansson[74], X. Kui[1], S. Kabana[33], N. Kalantar-Nayestanaki[63], X.L. Kang[10], X.S. Kang[40], R. Kappert[63], M. Kavatsyuk[63], B.C. Ke[80], A. Khoukaz[67], R. Kiuchi[1], R. Kliemt[14], O.B. Kolcu[61A], B. Kopf[4], M. Kuessner[4], A. Kupsc[44,74], W. Kühn[37], J.J. Lane[66], P. Larin[18], A. Lavania[26], L. Lavezzi[73A,73C], T.T. Lei[70,k], Z.H. Lei[70,57], H. Leithoff[35], M. Lellmann[35], T. Lenz[35], C. Li[47], C. Li[43], C.H. Li[39], Cheng Li[70,57], D.M. Li[80], F. Li[1,57], G. Li[1], H. Li[70,57], H.B. Li[1,62], H.J. Li[19], H.N. Li[55,i], Hui Li[43], J.R. Li[60], J.S. Li[58], J.W. Li[49], K.L. Li[19], Ke Li[1], L. J Li[1,62], L.K. Li[1], Lei Li[3], M.H. Li[43], P.R. Li[38,j,k], Q.X. Li[49], S.X. Li[13], T. Li[49], W.D. Li[1,62], W.G. Li[1], X.H. Li[70,57], X.L. Li[49], Xiaoyu Li[1,62], Y.G. Li[46,g], Z.J. Li[58], C. Liang[42], H. Liang[1,62], H. Liang[70,57], H. Liang[34], Y.F. Liang[53], Y.T. Liang[31,62], G.R. Liao[15], L.Z. Liao[49], Y.P. Liao[1,62], J. Libby[26], A. Limphirat[59], D.X. Lin[31,62], T. Lin[1], B.J. Liu[1], B.X. Liu[75], C. Liu[34], C.X. Liu[1], F.H. Liu[52], Fang Liu[1], Feng Liu[7], G.M. Liu[55,i], H. Liu[38,j,k], H.M. Liu[1,62], Huanhuan Liu[1], Huihui Liu[21], J.B. Liu[70,57], J.L. Liu[71], J.Y. Liu[1,62], K. Liu[1], K.Y. Liu[40], Ke Liu[22], L. Liu[70,57], L.C. Liu[43], Lu Liu[43], M.H. Liu[13,f], P.L. Liu[1], Q. Liu[62], S.B. Liu[70,57], T. Liu[13,f], W.K. Liu[43], W.M. Liu[70,57], X. Liu[38,j,k], Y. Liu[38,j,k], Y. Liu[80], Y.B. Liu[43], Z.A. Liu[1,57,62], Z.Q. Liu[49], X.C. Lou[1,57,62], F.X. Lu[58], H.J. Lu[23], J.G. Lu[1,57], X.L. Lu[1], Y. Lu[8], Y.P. Lu[1,57], Z.H. Lu[1,62], C.L. Luo[41], M.X. Luo[79], T. Luo[13,f], X.L. Luo[1,57], X.R. Lyu[62], Y.F. Lyu[43], F.C. Ma[40], H.L. Ma[1],

J.L. Ma[1,62], L.L. Ma[49], M.M. Ma[1,62], Q.M. Ma[1], R.Q. Ma[1,62], R.T. Ma[62], X.Y. Ma[1,57], Y. Ma[46,g], Y.M. Ma[31], F.E. Maas[18], M. Maggiora[73A,73C], S. Malde[68], Q.A. Malik[72], A. Mangoni[28B], Y.J. Mao[46,g], Z.P. Mao[1], S. Marcello[73A,73C], Z.X. Meng[65], J.G. Messchendorp[14,63], G. Mezzadri[29A], H. Miao[1,62], T.J. Min[42], R.E. Mitchell[27], X.H. Mo[1,57,62], N. Yu. Muchnoi[5,b], J. Muskalla[35], Y. Nefedov[36], F. Nerling[18,d], I.B. Nikolaev[5,b], Z. Ning[1,57], S. Nisar[12,l], Y. Niu [49], S.L. Olsen[62], Q. Ouyang[1,57,62], S. Pacetti[28B,28C], X. Pan[54], Y. Pan[56], A. Pathak[34], P. Patteri[28A], Y.P. Pei[70,57], M. Pelizaeus[4], H.P. Peng[70,57], K. Peters[14,d], J.L. Ping[41], R.G. Ping[1,62], S. Plura[35], S. Pogodin[36], V. Prasad[33], F.Z. Qi[1], H. Qi[70,57], H.R. Qi[60], M. Qi[42], T.Y. Qi[13,f], S. Qian[1,57], W.B. Qian[62], C.F. Qiao[62], J.J. Qin[71], L.Q. Qin[15], X.P. Qin[13,f], X.S. Qin[49], Z.H. Qin[1,57], J.F. Qiu[1], S.Q. Qu[60], C.F. Redmer[35], K.J. Ren[39], A. Rivetti[73C], V. Rodin[63], M. Rolo[73C], G. Rong[1,62], Ch. Rosner[18], S.N. Ruan[43], N. Salone[44], A. Sarantsev[36,c], Y. Schelhaas[35], K. Schoenning[74], M. Scodeggio[29A,29B], K.Y. Shan[13,f], W. Shan[24], X.Y. Shan[70,57], J.F. Shangguan[54], L.G. Shao[1,62], M. Shao[70,57], C.P. Shen[13,f], H.F. Shen[1,62], W.H. Shen[62], X.Y. Shen[1,62], B.A. Shi[62], H.C. Shi[70,57], J.L. Shi[13], J.Y. Shi[1], Q.Q. Shi[54], R.S. Shi[1,62], X. Shi[1,57], J.J. Song[19], T.Z. Song[58], W.M. Song[34,1], Y.J. Song[13], Y.X. Song[46,g], S. Sosio[73A,73C], S. Spataro[73A,73C], F. Stieler[35], Y.J. Su[62], G.B. Sun[75], G.X. Sun[1], H. Sun[62], H.K. Sun[1], J.F. Sun[19], K. Sun[60], L. Sun[75], S.S. Sun[1,62], T. Sun[1,62], W.Y. Sun[34], Y. Sun[10], Y.J. Sun[70,57], Y.Z. Sun[1], Z.T. Sun[49], Y.X. Tan[70,57], C.J. Tang[53], G.Y. Tang[1], J. Tang[58], Y.A. Tang[75], L. Y Tao[71], Q.T. Tao[25,h], M. Tat[68], J.X. Teng[70,57], V. Thoren[74], W.H. Tian[58], W.H. Tian[51], Y. Tian[31,62], Z.F. Tian[75], I. Uman[61B], S.J. Wang[49], B. Wang[1], B.L. Wang[62], Bo Wang[70,57], C.W. Wang[42], D.Y. Wang[46,g], F. Wang[71], H.J. Wang[38,j,k], H.P. Wang[1,62], J.P. Wang [49], K. Wang[1,57], L.L. Wang[1], M. Wang[49], Meng Wang[1,62], S. Wang[13,f], S. Wang[38,j,k], T. Wang[13,f], T.J. Wang[43], W. Wang[58], W. Wang[71], W.P. Wang[70,57], X. Wang[46,g], X.F. Wang[38,j,k], X.J. Wang[39], X.L. Wang[13,f], Y. Wang[60], Y.D. Wang[45], Y.F. Wang[1,57,62], Y.H. Wang[47], Y.N. Wang[45], Y.Q. Wang[1], Yaqian Wang[17,1], Yi Wang[60], Z. Wang[1,57], Z.L. Wang[71], Z.Y. Wang[1,62], Ziyi Wang[62], D. Wei[69], D.H. Wei[15], F. Weidner[67], S.P. Wen[1], C.W. Wenzel[4], U. Wiedner[4], G. Wilkinson[68], M. Wolke[74], L. Wollenberg[4], C. Wu[39], J.F. Wu[1,62], L.H. Wu[1], L.J. Wu[1,62], X. Wu[13,f], X.H. Wu[34], Y. Wu[70], Y.J. Wu[31], Z. Wu[1,57], L. Xia[70,57], X.M. Xian[39], T. Xiang[46,g], D. Xiao[38,j,k], G.Y. Xiao[42], S.Y. Xiao[1], Y.L. Xiao[13,f], Z.J. Xiao[41], C. Xie[42], X.H. Xie[46,g], Y. Xie[49], Y.G. Xie[1,57], Y.H. Xie[7], Z.P. Xie[70,57], T.Y. Xing[1,62], C.F. Xu[1,62], C.J. Xu[58], G.F. Xu[1], H.Y. Xu[65], Q.J. Xu[16], Q.N. Xu[30], W. Xu[1,62], W.L. Xu[65], X.P. Xu[54], Y.C. Xu[77], Z.P. Xu[42], Z.S. Xu[62], F. Yan[13,f], L. Yan[13,f], W.B. Yan[70,57], W.C. Yan[80], X.Q. Yan[1], H.J. Yang[50,e], H.L. Yang[34], H.X. Yang[1], Tao Yang[1], Y. Yang[13,f], Y.F. Yang[43], Y.X. Yang[1,62], Yifan Yang[1,62], Z.W. Yang[38,j,k], Z.P. Yao[49], M. Ye[1,57], M.H. Ye[9], J.H. Yin[1], Z.Y. You[58], B.X. Yu[1,57,62], C.X. Yu[43], G. Yu[1,62], J.S. Yu[25,h], T. Yu[71], X.D. Yu[46,g], C.Z. Yuan[1,62], L. Yuan[2], S.C. Yuan[1], X.Q. Yuan[1], Y. Yuan[1,62], Z.Y. Yuan[58], C.X. Yue[39], A.A. Zafar[72], F.R. Zeng[49], X. Zeng[13,f], Y. Zeng[25,h], Y.J. Zeng[1,62], X.Y. Zhai[34], Y.C. Zhai[49], Y.H. Zhan[58], A.Q. Zhang[1,62], B.L. Zhang[1,62], B.X. Zhang[1], D.H. Zhang[43], G.Y. Zhang[19], H. Zhang[70], H.H. Zhang[58], H.H. Zhang[34], H.Q. Zhang[1,57,62], H.Y. Zhang[1,57], J. Zhang[80], J.J. Zhang[51], J.L. Zhang[20], J.Q. Zhang[41], J.W. Zhang[1,57,62], J.X. Zhang[38,j,k], J.Y. Zhang[1], J.Z. Zhang[1,62], Jianyu Zhang[62], Jiawei Zhang[1,62], L.M. Zhang[60], L.Q. Zhang[58], Lei Zhang[42], P. Zhang[1,62], Q.Y. Zhang[39,80], Shuihan Zhang[1,62], Shulei Zhang[25,h], X.D. Zhang[45], X.M. Zhang[1], X.Y. Zhang[49], Xuyan Zhang[54], Y. Zhang[71], Y. Zhang[68], Y.T. Zhang[80], Y.H. Zhang[1,57], Yan Zhang[70,57], Yao Zhang[1], Z.H. Zhang[1], Z.L. Zhang[34], Z.Y. Zhang[75], Z.Y. Zhang[43], G. Zhao[1], J. Zhao[39], J.Y. Zhao[1,62], J.Z. Zhao[1,57], Lei Zhao[70,57],

Ling Zhao[1], M.G. Zhao[43], S.J. Zhao[80], Y.B. Zhao[1,57], Y.X. Zhao[31,62], Z.G. Zhao[70,57], A. Zhemchugov[36,a], B. Zheng[71], J.P. Zheng[1,57], W.J. Zheng[1,62], Y.H. Zheng[62], B. Zhong[41], X. Zhong[58], H. Zhou[49], L.P. Zhou[1,62], X. Zhou[75], X.K. Zhou[7], X.R. Zhou[70,57], X.Y. Zhou[39], Y.Z. Zhou[13,f], J. Zhu[43], K. Zhu[1], K.J. Zhu[1,57,62], L. Zhu[34], L.X. Zhu[62], S.H. Zhu[69], S.Q. Zhu[42], T.J. Zhu[13,f], W.J. Zhu[13,f], Y.C. Zhu[70,57], Z.A. Zhu[1,62], J.H. Zou[1], J. Zu[70,57]

[1] *Institute of High Energy Physics, Beijing 100049, People's Republic of China*
[2] *Beihang University, Beijing 100191, People's Republic of China*
[3] *Beijing Institute of Petrochemical Technology, Beijing 102617, People's Republic of China*
[4] *Bochum Ruhr-University, D-44780 Bochum, Germany*
[5] *Budker Institute of Nuclear Physics SB RAS (BINP), Novosibirsk 630090, Russia*
[6] *Carnegie Mellon University, Pittsburgh, Pennsylvania 15213, U.S.A.*
[7] *Central China Normal University, Wuhan 430079, People's Republic of China*
[8] *Central South University, Changsha 410083, People's Republic of China*
[9] *China Center of Advanced Science and Technology, Beijing 100190, People's Republic of China*
[10] *China University of Geosciences, Wuhan 430074, People's Republic of China*
[11] *Chung-Ang University, Seoul, 06974, Republic of Korea*
[12] *COMSATS University Islamabad, Lahore Campus, Defence Road, Off Raiwind Road, 54000 Lahore, Pakistan*
[13] *Fudan University, Shanghai 200433, People's Republic of China*
[14] *GSI Helmholtzcentre for Heavy Ion Research GmbH, D-64291 Darmstadt, Germany*
[15] *Guangxi Normal University, Guilin 541004, People's Republic of China*
[16] *Hangzhou Normal University, Hangzhou 310036, People's Republic of China*
[17] *Hebei University, Baoding 071002, People's Republic of China*
[18] *Helmholtz Institute Mainz, Staudinger Weg 18, D-55099 Mainz, Germany*
[19] *Henan Normal University, Xinxiang 453007, People's Republic of China*
[20] *Henan University, Kaifeng 475004, People's Republic of China*
[21] *Henan University of Science and Technology, Luoyang 471003, People's Republic of China*
[22] *Henan University of Technology, Zhengzhou 450001, People's Republic of China*
[23] *Huangshan College, Huangshan 245000, People's Republic of China*
[24] *Hunan Normal University, Changsha 410081, People's Republic of China*
[25] *Hunan University, Changsha 410082, People's Republic of China*
[26] *Indian Institute of Technology Madras, Chennai 600036, India*
[27] *Indiana University, Bloomington, Indiana 47405, U.S.A.*
[28] *INFN Laboratori Nazionali di Frascati, (A)INFN Laboratori Nazionali di Frascati, I-00044, Frascati, Italy; (B)INFN Sezione di Perugia, I-06100, Perugia, Italy; (C)University of Perugia, I-06100, Perugia, Italy*
[29] *INFN Sezione di Ferrara, (A)INFN Sezione di Ferrara, I-44122, Ferrara, Italy; (B)University of Ferrara, I-44122, Ferrara, Italy*
[30] *Inner Mongolia University, Hohhot 010021, People's Republic of China*
[31] *Institute of Modern Physics, Lanzhou 730000, People's Republic of China*
[32] *Institute of Physics and Technology, Peace Avenue 54B, Ulaanbaatar 13330, Mongolia*
[33] *Instituto de Alta Investigación, Universidad de Tarapacá, Casilla 7D, Arica 1000000, Chile*
[34] *Jilin University, Changchun 130012, People's Republic of China*
[35] *Johannes Gutenberg University of Mainz, Johann-Joachim-Becher-Weg 45, D-55099 Mainz, Germany*
[36] *Joint Institute for Nuclear Research, 141980 Dubna, Moscow region, Russia*
[37] *Justus-Liebig-Universitaet Giessen, II. Physikalisches Institut, Heinrich-Buff-Ring 16, D-35392 Giessen, Germany*
[38] *Lanzhou University, Lanzhou 730000, People's Republic of China*
[39] *Liaoning Normal University, Dalian 116029, People's Republic of China*
[40] *Liaoning University, Shenyang 110036, People's Republic of China*
[41] *Nanjing Normal University, Nanjing 210023, People's Republic of China*

[42] *Nanjing University, Nanjing 210093, People's Republic of China*

[43] *Nankai University, Tianjin 300071, People's Republic of China*

[44] *National Centre for Nuclear Research, Warsaw 02-093, Poland*

[45] *North China Electric Power University, Beijing 102206, People's Republic of China*

[46] *Peking University, Beijing 100871, People's Republic of China*

[47] *Qufu Normal University, Qufu 273165, People's Republic of China*

[48] *Shandong Normal University, Jinan 250014, People's Republic of China*

[49] *Shandong University, Jinan 250100, People's Republic of China*

[50] *Shanghai Jiao Tong University, Shanghai 200240, People's Republic of China*

[51] *Shanxi Normal University, Linfen 041004, People's Republic of China*

[52] *Shanxi University, Taiyuan 030006, People's Republic of China*

[53] *Sichuan University, Chengdu 610064, People's Republic of China*

[54] *Soochow University, Suzhou 215006, People's Republic of China*

[55] *South China Normal University, Guangzhou 510006, People's Republic of China*

[56] *Southeast University, Nanjing 211100, People's Republic of China*

[57] *State Key Laboratory of Particle Detection and Electronics, Beijing 100049, Hefei 230026, People's Republic of China*

[58] *Sun Yat-Sen University, Guangzhou 510275, People's Republic of China*

[59] *Suranaree University of Technology, University Avenue 111, Nakhon Ratchasima 30000, Thailand*

[60] *Tsinghua University, Beijing 100084, People's Republic of China*

[61] *Turkish Accelerator Center Particle Factory Group, (A)Istinye University, 34010, Istanbul, Turkey; (B)Near East University, Nicosia, North Cyprus, 99138, Mersin 10, Turkey*

[62] *University of Chinese Academy of Sciences, Beijing 100049, People's Republic of China*

[63] *University of Groningen, NL-9747 AA Groningen, The Netherlands*

[64] *University of Hawaii, Honolulu, Hawaii 96822, U.S.A.*

[65] *University of Jinan, Jinan 250022, People's Republic of China*

[66] *University of Manchester, Oxford Road, Manchester, M13 9PL, United Kingdom*

[67] *University of Muenster, Wilhelm-Klemm-Strasse 9, 48149 Muenster, Germany*

[68] *University of Oxford, Keble Road, Oxford OX13RH, United Kingdom*

[69] *University of Science and Technology Liaoning, Anshan 114051, People's Republic of China*

[70] *University of Science and Technology of China, Hefei 230026, People's Republic of China*

[71] *University of South China, Hengyang 421001, People's Republic of China*

[72] *University of the Punjab, Lahore-54590, Pakistan*

[73] *University of Turin and INFN, (A)University of Turin, I-10125, Turin, Italy; (B)University of Eastern Piedmont, I-15121, Alessandria, Italy; (C)INFN, I-10125, Turin, Italy*

[74] *Uppsala University, Box 516, SE-75120 Uppsala, Sweden*

[75] *Wuhan University, Wuhan 430072, People's Republic of China*

[76] *Xinyang Normal University, Xinyang 464000, People's Republic of China*

[77] *Yantai University, Yantai 264005, People's Republic of China*

[78] *Yunnan University, Kunming 650500, People's Republic of China*

[79] *Zhejiang University, Hangzhou 310027, People's Republic of China*

[80] *Zhengzhou University, Zhengzhou 450001, People's Republic of China*

[a] *Also at the Moscow Institute of Physics and Technology, Moscow 141700, Russia*

[b] *Also at the Novosibirsk State University, Novosibirsk, 630090, Russia*

[c] *Also at the NRC "Kurchatov Institute", PNPI, 188300, Gatchina, Russia*

[d] *Also at Goethe University Frankfurt, 60323 Frankfurt am Main, Germany*

[e] *Also at Key Laboratory for Particle Physics, Astrophysics and Cosmology, Ministry of Education; Shanghai Key Laboratory for Particle Physics and Cosmology; Institute of Nuclear and Particle Physics, Shanghai 200240, People's Republic of China*

[f] *Also at Key Laboratory of Nuclear Physics and Ion-beam Application (MOE) and Institute of Modern Physics, Fudan University, Shanghai 200443, People's Republic of China*

^{g} Also at State Key Laboratory of Nuclear Physics and Technology, Peking University, Beijing 100871, People's Republic of China

^{h} Also at School of Physics and Electronics, Hunan University, Changsha 410082, China

^{i} Also at Guangdong Provincial Key Laboratory of Nuclear Science, Institute of Quantum Matter, South China Normal University, Guangzhou 510006, China

^{j} Also at Frontiers Science Center for Rare Isotopes, Lanzhou University, Lanzhou 730000, People's Republic of China

^{k} Also at Lanzhou Center for Theoretical Physics, Key Laboratory of Theoretical Physics of Gansu Province, and Key Laboratory for Quantum Theory and Applications of MoE, Lanzhou University, Lanzhou 730000, People's Republic of China

^{l} Also at the Department of Mathematical Sciences, IBA, Karachi 75270, Pakistan